Power Quality Enhancement of a Multi-Functional Grid-Tied PV System using an ANN-Controlled Split-Source Inverter

Girugula Kaveri[1], Rudroju Mounika[2*]

[1]PG Student, [2]Assistant Professor, [1,2]Department of Electrical and Electronics Engineering

[1,2]Vaagdevi College of Engineering (UGC-Autonomous), Bollikunta, Warangal, 506005, Telangana

[1]kaverigirugula@gmail.com, [2]rudrojumounika@gmail.com

*Correspondence: Rudroju Mounika (rudrojumounika@gmail.com)

Abstract

As global renewable energy capacity surpasses 4 TW, power quality challenges such as harmonic distortion, reactive power demands, and voltage instability threaten modern grid-tied solar photovoltaic (PV) networks. Mitigating these issues while ensuring grid compliance under nonlinear loads requires advanced power conversion and control strategies. However, traditional grid-connected PV systems utilizing standard Integral Sliding Mode Controllers (ISMC) suffer from sluggish dynamic responses, DC-link voltage fluctuations, and high total harmonic distortion (THD). To overcome these limitations, this paper proposes an Artificial Neural Network (ANN)-based Sliding Mode Controlled Split-Source Inverter (SSI) featuring integrated reactive power compensation and harmonic suppression. The ANN architecture dynamically processes grid voltages and currents to generate optimized reference signals. Concurrently, a dual-stage Sliding Mode Control (SMC) framework regulates the DC-link voltage on the DC side while ensuring precise current tracking and harmonic mitigation on the AC side via a Modified Space Vector Modulation (MSVM) technique. Performance evaluations demonstrate that the coordinated ANN–SMC framework significantly minimizes THD, stabilizes DC-link voltage, and superiorly enhances grid resilience under volatile operating conditions.

Keywords: Modified Space Vector Modulation (MSVM), Sliding Mode Controller (SMC), Integral Sliding Mode Controller (ISMC), Split-Source Inverter (SSI), photovoltaic (PV).

1. Introduction

The global transition toward clean and sustainable energy systems has accelerated significantly over the last decade due to increasing electricity demand, depletion of fossil fuel resources, and growing environmental concerns. According to international energy reports, renewable energy sources contribute an increasingly larger share of global electricity generation, with solar photovoltaic (PV) technology emerging as one of the fastest-growing energy sectors. The worldwide installed solar PV capacity has surpassed several terawatts and continues to expand due to declining installation costs, government incentives, and advancements in power electronic converters. In parallel, modern electrical networks are experiencing a rapid increase in nonlinear loads such as variable-speed drives, electric vehicle chargers, switched-mode power supplies, industrial automation equipment, and data center infrastructures. These loads introduce harmonics, reactive power consumption, voltage fluctuations, and power quality issues that negatively affect grid stability and operational efficiency. As a result, utility operators and industrial facilities are increasingly focusing on technologies that can simultaneously support renewable energy integration and maintain acceptable power quality standards.

Figure 1 presents a comparative illustration of the conventional power grid and the smart grid architecture in the context of MFGC based renewable energy systems. The traditional grid operates through a centralized power generation model, where electricity is produced by a limited number of large power plants and delivered to consumers through extensive transmission and distribution networks. Power flow occurs in a unidirectional manner from generation units to end users, and consumers function only as electricity receivers. This architecture faces challenges such as transmission losses, limited flexibility, reduced renewable energy penetration, and difficulties in handling dynamic load variations.

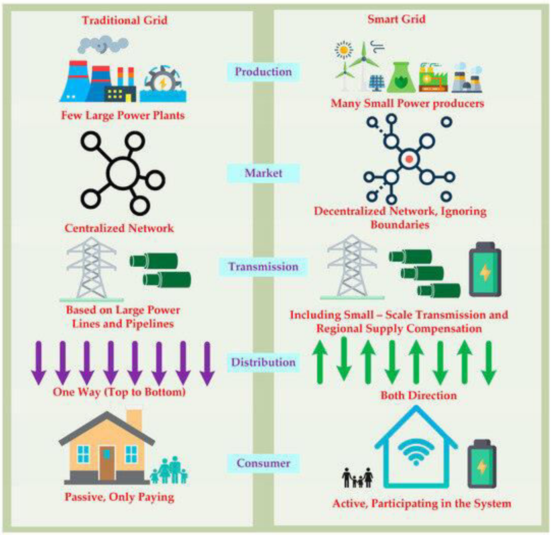

Figure 1. Comparison between conventional grid and smart grid architecture for MFGC based renewable energy systems.

1.1 Classification of MFGC based PV Inverter Topologies

The topology classification is broadly divided into Voltage Source Inverters (VSI) and Current Source Inverters (CSI). The voltage source category includes conventional multilevel inverter structures and two-level inverter configurations, while the current source category encompasses single DC source, boost current, multiple DC source, and dual current source inverter arrangements. This classification provides a systematic overview of the available inverter architectures employed in modern grid-connected PV systems for efficient power conversion and renewable energy integration.

Within the voltage source inverter category, multilevel inverter topologies are further classified into single DC source and multiple DC source configurations. Single DC source structures include Flying Capacitor (FC), Neutral Point Clamped (NPC), Active Neutral Point Clamped (ANPC), Hybrid Neutral Point Clamped (HNPC), Magnetic Coupled, Diode Clamped with Second Capacitive Divider, Full Bridge with Ancillary Circuit, and T-Type inverters. Multiple DC source topologies comprise Dual Voltage Source, Assisted Modular, Cascaded H-Bridge (CHB), Hybrid Full Bridge, and Modular Multilevel Converter (MMC) structures, which can operate with either equal or unequal DC sources. These architectures can be further implemented using single delta bridge cells, single star bridge cells, double star chopper cells, and double star bridge cells. Owing to their superior voltage quality, reduced harmonic distortion, lower switching stress, and enhanced scalability, multilevel inverter topologies have become a key enabling technology for high-performance grid-connected photovoltaic energy systems.

2. Literature Survey

A. Array-Level Optimization: Partial Shading, Mitigation, and Stability

Maximal energy extraction from photovoltaic (PV) installations requires addressing non-uniform environmental factors and control system stability. Dhimish and Badran [10] developed an active current-limiting circuit using operational amplifiers and MOSFET devices to mitigate the adverse effects of partial shading and hot-spot development within mismatched PV sub-strings. Unlike traditional bypass diodes, which fail to lower cell temperatures effectively, their solution clamped excessive current to minimize thermal stress, drawing a negligible power dissipation of 0.53 W while improving module lifetime. The relationship between physical cell connections and shading profiles was evaluated by Oguz *et al.* [11]. Testing eight array configurations across six shading distributions and three maximum power point tracking (MPPT) techniques on a DSP platform, they demonstrated that Total Cross-Tied (TCT) interconnections consistently yielded the highest power extraction under all shading profiles.

At the grid interface level, nonlinear controller interactions can introduce unexpected destabilization. Rahman and Mohamed [9] conducted a describing function (DF)-based analytical stability investigation of a single-stage grid-connected PV system using the Incremental Conductance (INC) MPPT algorithm. Their time-domain modeling revealed that low DC-link capacitance, small AC-side filter inductances, and operations away from the maximum power point (MPP) aggravate system oscillations. To counter this, they implemented an active compensation technique that significantly suppresses transient fluctuations under volatile operating states.

B. Multilevel Transformerless and Fault-Tolerant Inverter Topologies

To reduce installation costs, volume, and weight while maximizing efficiency, transformerless topologies have become prominent. Faraji *et al.* [12] presented an extensive review of single-stage, single-phase, three-level neutral-point-clamped (3L-NPC) transformerless inverters. By examining over forty-five configurations within the three-level family, the authors modeled common-mode current loops to analyze leakage-current characteristics, component count, and modulation metrics, establishing the 3L-NPC framework as an efficient and practical solution for high-performance grid-tied arrays.

To improve voltage resolution and reduce harmonic distortion, high-level configurations are increasingly explored. Laib *et al.* [2] introduced a single-phase thirteen-level Packed E-Cell (PEC13) inverter employing six conventional switches, two four-quadrant switches, and four DC capacitors. Their design featured an inherent fault-tolerant framework managed by a reconfigurable finite-control-set model predictive control (R-FCS-MPC) scheme. In the event of an open-circuit fault in the four-quadrant switches, the system automatically reconfigures into PEC9 or PUC7 operating modes without supplementary hardware, maintaining smooth capacitor voltage balance and continuous grid integration under varying irradiances.

Similarly, Sahli *et al.* [7] proposed a modified five-level Packed U-Cell (MPUC5) topology for a single-phase, double-stage grid-connected system operating at unity power factor. Utilizing a six-switch architecture with two DC-link capacitors tied to an intermediate Cúk DC–DC converter for MPPT, their framework used FCS-MPC to track grid currents and balance capacitor voltages while simultaneously providing active power filtering against nonlinear local loads.

C. Multifunctional Grid Integration and Coordinated Energy Management

Modern grid standards require grid-connected inverters to operate beyond simple real-power injectors. Zeng *et al.* [3] performed a detailed evaluation of multifunctional grid-connected inverters (MFGCIs) operating within distributed networks and microgrids. The authors demonstrated that MFGCIs serve as crucial structural nodes for reactive power support, active harmonic compensation, and voltage disturbance mitigation, balancing the technical challenges imposed by volatile renewable generation. Advanced control strategies have been developed to regulate these multi-objective setups. Krama *et al.* [4] formulated a two-stage grid-connected control framework utilizing Model Predictive Power Control combined with Space Vector Modulation (MPPC-SVM) to minimize active and reactive power tracking deviations. Supported by a Sliding Mode Control-based Particle Swarm Optimization (SMC-PSO) MPPT routine and an optimized anti-windup PI DC-link controller, their setup delivered clean sinusoidal currents with active filtering features without needing discrete harmonic extraction algorithms.

For single-stage architectures, Libo *et al.* [6] developed a three-phase system using an enhanced incremental conductance tracking approach implemented on a Digital Signal Processor (DSP), providing localized reactive power support to offload the utility grid. When priority management is crucial due to inverter thermal boundaries, Soumana *et al.* [5] proposed an Adaptive Neuro-Fuzzy Inference System (ANFIS) MPPT structure operating alongside a two-phase interleaved boost converter and a 3L-NPC inverter. Their control logic systematically prioritized active power generation first, followed by reactive compensation and harmonic mitigation according to the remaining thermal capacity of the switches, yielding a 16.95% improvement in total harmonic distortion (THD) over classical architectures. To ensure continuous system reliability when solar power is absent, Myneni and Ganjikunta [8] introduced a coordinated energy-management loop pairing a single-stage voltage source converter with a bidirectional DC–DC battery charging circuit. Their controller monitors battery state-of-charge (SOC) to regulate power flow and rectify neutral-current imbalances, incorporating an active rectification mode that repurposes the inverter as a grid-supportive static var compensator during zero-irradiance periods.

D. Impedance-Source Inverter (ISI) Architectures

Traditional two-stage conversion architectures often incur high switching losses due to cascading topologies. To address this, Jamal *et al.* [1] conducted a comprehensive review of impedance-source inverter (ISI) systems, showing how single-stage impedance networks eliminate the need for distinct step-up DC–DC converters while boosting efficiency and tracking robustness. This single-stage buck-boost concept originated with the Z-source inverter (ZSI) proposed by Peng [13]. By integrating a unique symmetric X-shaped LC impedance network between the power source and the inverter bridge, the ZSI exploits the shoot-through zero states—which would short-circuit and destroy conventional voltage-source inverters—to achieve single-stage voltage amplification, as successfully demonstrated in fuel-cell configurations. To improve upon the ZSI topology, Li *et al.* [14] developed a comprehensive modeling and control framework for the quasi-Z-source inverter (qZSI). Through small-signal modeling and state-space averaging, they designed a constant capacitor-voltage control strategy that decouples the modulation index from the shoot-through duty ratio, effectively minimizing switch voltage stress and delivering reliable voltage regulation for grid-connected distributed generation systems.

3. Proposed System

Figure 2 illustrates the complete architecture of the proposed MFGC based photovoltaic system employing an ANN-based controller and SSI. The system consists of a three-phase utility grid, nonlinear load, ANN controller, split-source inverter, DC-link capacitor, input inductor, and PV array. The ANN controller continuously monitors system variables including load current, filter current, grid voltage, and DC-link voltage to generate optimal switching commands for the inverter. The generated switching signals regulate power flow between the PV source and utility grid while maintaining DC-link voltage stability, compensating harmonics, improving power factor, and ensuring high-quality power delivery at the PCC. Through adaptive learning and nonlinear mapping capabilities, the ANN controller effectively handles system uncertainties, load disturbances, and renewable energy intermittency, resulting in superior dynamic performance, reduced harmonic distortion, enhanced voltage regulation, and improved grid integration capability.

Three-Phase Grid Voltage Generation: The utility grid supplies balanced three-phase voltages to the system. The grid voltage acts as the primary reference source for synchronization and power exchange. The grid-side inductance and resistance represent the transmission network impedance. The instantaneous three-phase voltages are represented as:

$$v_{ga} = V_m sin\,(\omega t) \tag{3.1}$$

$$v_{gb} = V_m sin\left(\frac{2\pi}{3}\right) \tag{3.2}$$

$$v_{gc} = V_m sin\left(\frac{2\pi}{3}\right) \tag{3.3}$$

Here, $V_m$is the peak voltage and ωdenotes the angular frequency. These voltages establish the reference framework for synchronization and current control. The ANN controller utilizes the grid voltage information to determine the system operating condition and maintain synchronization with the utility network. Accurate voltage measurement enables proper power injection and stable inverter operation under varying grid conditions.

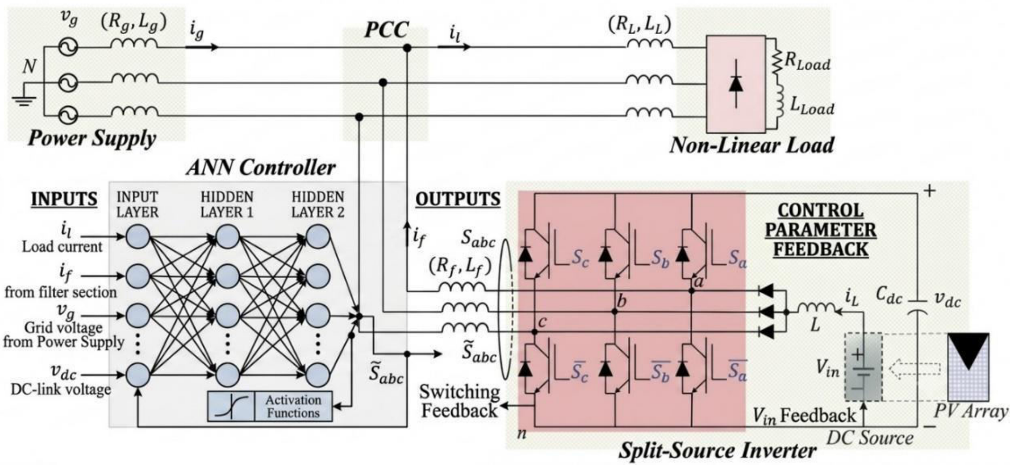

Figure 2. Complete MFGC system with ANN-based control for SSI.

PCC Monitoring: The Point of Common Coupling serves as the interconnection node between the utility grid, inverter, and nonlinear load. All power exchange occurs through this point. The current relationship at PCC follows Kirchhoff's Current Law:

$$i_g = i_L - i_f \tag{3.4}$$

Here, $i_g$represents source current, $i_L$denotes load current, and $i_f$corresponds to filter current injected by the inverter. The PCC voltage remains a critical parameter for maintaining grid stability. Continuous monitoring of PCC conditions enables effective harmonic compensation and reactive power support. The ANN controller processes PCC information to determine the required compensation current. This ensures sinusoidal source current and stable voltage conditions despite load disturbances.

Nonlinear Load Current Extraction: The nonlinear load draws distorted current containing harmonic components. The load current can be expressed as:

$$i_L = i_{L1} + i_{Lh} \tag{3.5}$$

Here, $i_{L1}$is the fundamental component and i_{Lh}represents harmonic currents. These harmonics degrade power quality and increase system losses. The ANN controller receives the measured load current and identifies compensation requirements. By analyzing the harmonic content and dynamic load behavior, the controller generates appropriate switching actions. This process enables harmonic mitigation and maintains grid current quality within standard limits.

PV Array Power Generation: The photovoltaic array converts solar energy into electrical energy and acts as the primary DC source. The PV output power is given by:

$$P_{PV} = V_{PV} I_{PV} \tag{3.6}$$

Here, $V_{PV}$and I_{PV}denote PV voltage and current respectively. The generated power varies according to solar irradiance and temperature. The PV source supplies energy to the split-source inverter for grid integration. Continuous power extraction improves renewable energy utilization. The ANN controller adapts to changing PV conditions and maintains stable operation despite environmental variations.

DC-Link Capacitor Voltage Regulation: The DC-link capacitor stores energy and stabilizes the inverter input voltage. The capacitor energy is expressed as:

$$E_{dc} = \frac{1}{2} C_{dc} V_{dc}^2 \tag{3.7}$$

where $C_{dc}$is the DC-link capacitance and V_{dc}represents capacitor voltage. Maintaining a constant DC-link voltage is essential for proper inverter operation. Voltage fluctuations directly affect output waveform quality. The ANN controller continuously monitors the DC-link voltage and adjusts inverter switching patterns to maintain voltage stability. This regulation improves transient response and enhances system reliability.

Input Inductor Energy Management: The split-source inverter employs an input inductor to achieve voltage boosting and energy transfer. The energy stored in the inductor is:

$$E_L = \frac{1}{2} L I_L^2 \tag{3.8}$$

Here, L denotes inductance and $I_L$is the inductor current. The inductor smooths current variations and supports boost operation. Proper inductor current control minimizes ripple and switching stress. The ANN controller observes current variations and dynamically adjusts inverter states. This results in efficient energy conversion and improved system performance.

ANN Input Layer Processing: The ANN controller receives measured system variables as input features:

$$X = [i_L,\ i_f,\ v_g,\ V_{dc}] \tag{3.9}$$

These parameters contain information regarding load demand, compensation current, grid condition, and energy status. The input layer normalizes the signals before forwarding them to hidden layers. ANN learning enables nonlinear mapping between system states and control actions. This adaptive capability allows accurate decision-making under varying operating conditions.

Hidden Layer Feature Extraction: The hidden layers perform nonlinear processing and feature extraction. The neuron output is calculated as:

$$h_j = f(b_j) \tag{3.10}$$

Here, w_{ij}denotes connection weights, $b_j$represents bias, and $f(\cdot)$is the activation function. Hidden layers identify complex relationships among system variables. The extracted features improve controller intelligence and prediction capability. This stage enables accurate estimation of required compensation currents and switching states.

ANN Output Layer and Switching Signal Generation: The ANN output layer generates inverter switching commands:

$$S_{abc} = ANN(X) \tag{3.11}$$

Here, S_{abc}represents switching signals for inverter switches. The controller determines the optimal switching state based on system conditions. The generated pulses regulate power flow, harmonic compensation, and voltage control. Intelligent switching reduces losses and improves dynamic response. The ANN continuously updates switching actions according to real-time operating conditions.

Split-Source Inverter Operation: The split-source inverter converts DC power into AC power while providing voltage boosting capability. The inverter output voltage can be represented as:

$$V_o = M\, V_{dc} \tag{3.12}$$

Here, Mdenotes the modulation index. The inverter synthesizes sinusoidal voltages using ANN-generated switching commands. The split-source structure eliminates the need for an additional DC–DC converter. This improves efficiency and reduces component count. The inverter injects compensating current into the PCC for power quality enhancement.

Filter Current Injection and Harmonic Compensation: The inverter injects compensation current through the filter inductance. The reference filter current is given by:

$$i_f^* = i_L - i_g^* \tag{3.13}$$

Here, i_g^*denotes the desired source current. The injected current cancels harmonic components drawn by the nonlinear load. As a result, source currents become sinusoidal and balanced. The ANN controller dynamically adjusts compensation current according to load variations. This improves overall power quality and reduces total harmonic distortion.

Grid Power Exchange and System Stabilization: The final stage involves regulated power exchange between the PV source, inverter, grid, and load. The active power transferred to the grid is expressed as:

$$P_g = v_g i_g \tag{3.14}$$

while reactive power is represented by:

$$Q_g = v_g i_q \tag{3.15}$$

The ANN controller maintains stable DC-link voltage, regulates power flow, minimizes harmonics, and improves power factor. Through intelligent learning and adaptive control, the proposed MFGC system achieves enhanced dynamic performance, superior power quality, efficient renewable energy utilization, and reliable grid-connected operation.

3.1 Proposed ANN-Based Control Scheme

Figure 3 illustrates the proposed ANN based control scheme employed in the MFGC photovoltaic system. The control architecture integrates an ANN control block, DC-side SMC, Grid-side SMC, PLL, coordinate transformation unit, and MSVM module. The ANN controller continuously monitors system variables such as DC-link voltage, load current, and grid conditions to generate an optimal reference current signal. The DC-side SMC maintains DC-link voltage stability and generates active current references, while the Grid-side SMC regulates compensation currents and produces reference voltage signals. The PLL provides accurate grid synchronization, and the MSVM module converts the controller outputs into inverter switching pulses. Through coordinated operation of these control blocks, the proposed system achieves effective harmonic compensation, improved current tracking, enhanced voltage regulation, reduced total harmonic distortion, and superior power quality at the PCC.

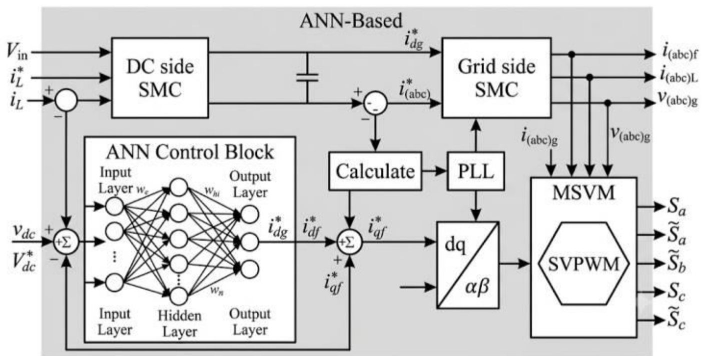

Figure 3. Proposed ANN-based control scheme.

3.2 Proposed DC-Side Sliding Mode Controller

Figure 4 illustrates the structure of the proposed DC-SMC employed in the ANN-based MFGC photovoltaic system. The primary objective of the DC-SMC is to regulate the DC-link voltage and generate the duty cycle signal required for controlling the SSI. The controller continuously compares the reference inductor current with the actual inductor current to establish a sliding surface that reflects the system error dynamics. The generated sliding variable is processed through a nonlinear control mechanism that incorporates a boundary layer parameter and adaptive gain to improve robustness and reduce chattering. Simultaneously, the controller considers the relationship between the DC-link voltage and input voltage to ensure proper voltage boosting and energy transfer. By combining current-tracking information with voltage regulation feedback, the DC-SMC produces an optimal duty cycle command for inverter operation. This control strategy provides fast dynamic response, strong disturbance rejection capability, stable DC-link voltage regulation, and enhanced power quality performance under varying load and renewable energy conditions.

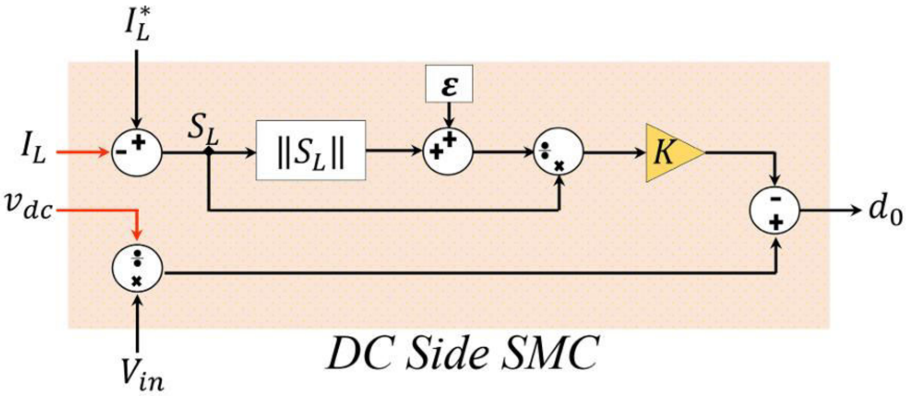

Figure 4. Block diagram of the proposed DC-SMC.

4. Results and discussion

Figure 5 presents the complete MATLAB/Simulink model of the proposed grid-connected photovoltaic system employing an ANN-based controller integrated with a Split-Source Inverter (SSI). The system consists of a PV array, split-source converter, DC-link capacitor, ANN control unit, three-phase inverter, coupling inductors, transformer interface, nonlinear load, and utility grid. The ANN controller continuously processes PV voltage, PV current, inverter voltage, and DC-link voltage information to generate optimized switching commands for the inverter. The proposed configuration enables efficient power transfer, improved voltage regulation, harmonic suppression, and reactive power compensation while maintaining stable operation under varying environmental and loading conditions.

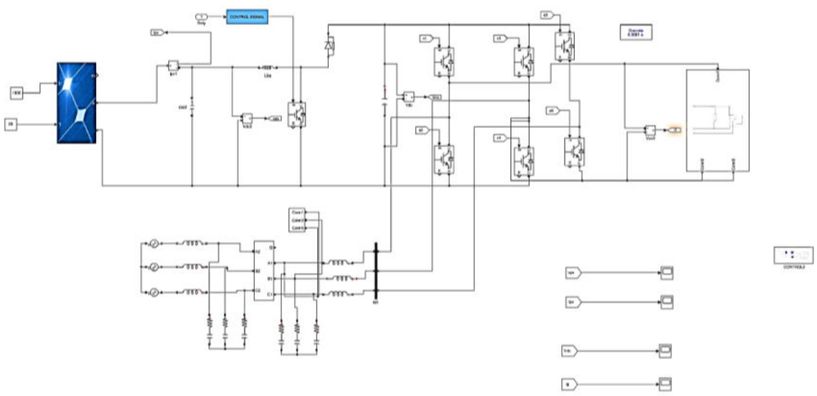

Figure 5. Overall Simulation Model of the Proposed ANN-Based SSI.

Figure 6 illustrates the ANN-based controller subsystem used in the proposed grid-connected PV system. The controller receives PV voltage, PV current, and inverter voltage signals as inputs and processes them through trained neural network structures to generate optimal control signals. Multiple ANN blocks are employed to regulate DC-link voltage, current tracking, and inverter switching operations. The generated outputs are supplied to pulse generation circuits, which produce gating signals $S_1$to $S_6$for inverter operation. The ANN controller provides adaptive learning capability, rapid response, and improved robustness compared with conventional control methods.

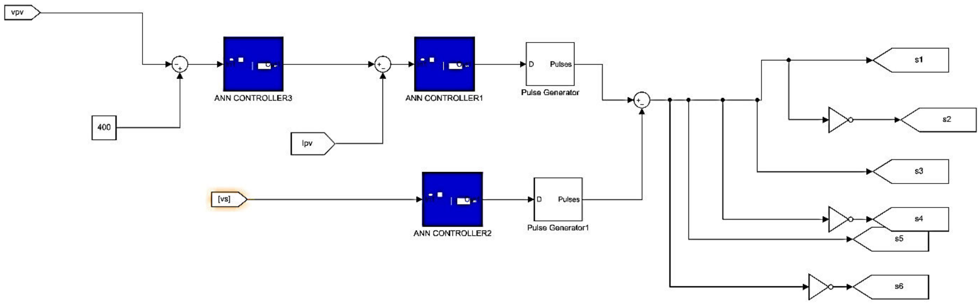

Figure 6. ANN Controller Subsystem of the Proposed System

Figure 7 depicts the photovoltaic array voltage profile under different operating conditions. The PV voltage remains approximately 900 V from 0 s to 1 s, increases sharply to approximately 2500 V between 1 s and 2 s, and subsequently decreases to nearly 0 V after 2 s. The waveform demonstrates the wide operating range of the photovoltaic source and the ability of the proposed ANN controller to accommodate significant variations in renewable energy generation while maintaining stable system operation. Figure 8 presents the PV current waveform corresponding to the changing PV operating conditions. Initially, the PV current remains approximately 18 A up to 0.5 s, gradually increases to 30 A at 1 s, remains constant at 30 A between 1 s and 2 s, and decreases to approximately 10 A after 2 s. These variations indicate changes in solar power generation conditions. The ANN controller successfully adapts to these changes and maintains stable power transfer throughout the operating period. Figure 9 illustrates the DC-link voltage regulation performance achieved using the proposed ANN controller. The DC-link voltage is maintained at a constant value of approximately 400 V throughout the entire simulation period from 0 s to 3 s. Unlike the existing Integral Sliding Mode Controller, which exhibited voltage oscillations and transient deviations, the proposed ANN controller completely eliminates voltage fluctuations and provides excellent voltage regulation performance. This demonstrates the superior dynamic response and adaptive control capability of the ANN-based approach.

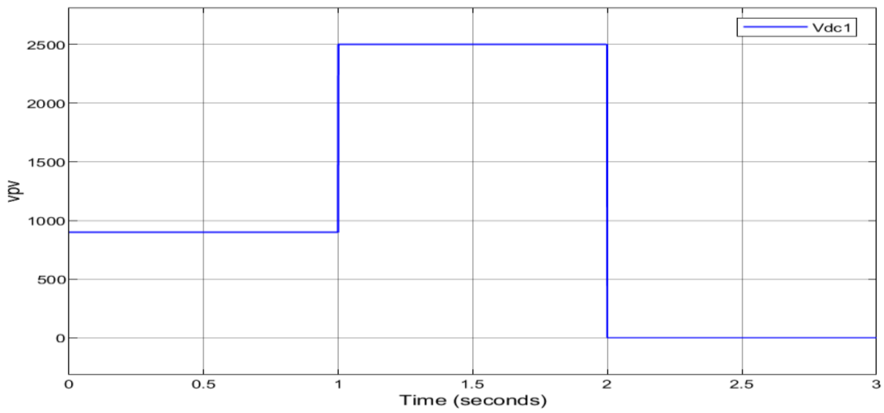

Figure 7. PV Voltage Characteristics of the Proposed System

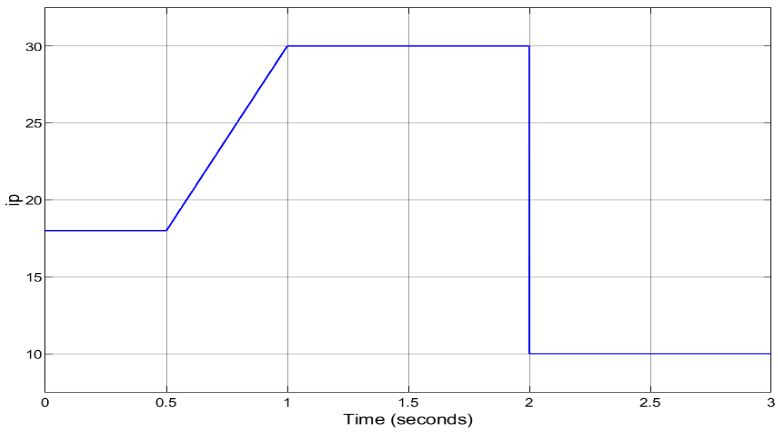

Figure 8. PV Current Characteristics of the Proposed System

Figure 10 shows the three-phase grid current waveforms injected into the utility network. During the interval from 0 s to approximately 1.1 s, the current amplitude remains around ±12 A. Between 1.1 s and 2 s, the amplitude decreases to approximately ±6 A, reflecting reduced power demand. After 2 s, the current returns to approximately ±12 A. The waveforms remain balanced and sinusoidal throughout the operating period, indicating effective current control and successful grid synchronization achieved by the ANN controller.

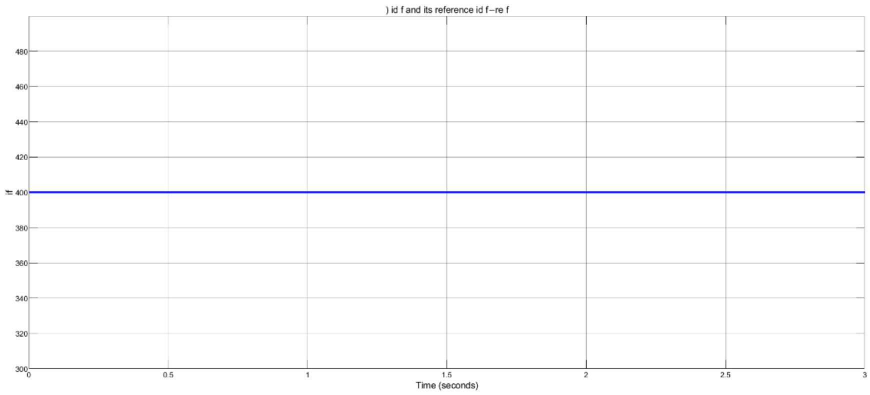

Figure 9. DC-Link Voltage Response of the Proposed ANN-Controlled System

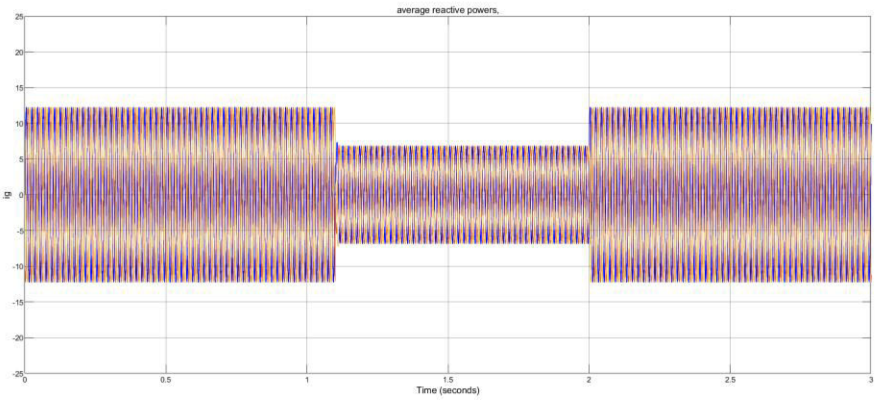

Figure 10. Grid Current Waveforms of the Proposed System

Figure 11 presents the FFT analysis of the grid current obtained using the proposed ANN-based controller. The fundamental component is measured as 12.24 A at 50 Hz, while the THD is reduced to only 0.34%. The harmonic spectrum shows extremely low magnitudes of higher-order frequency components, demonstrating the effectiveness of the ANN controller in suppressing current harmonics. Compared with the existing system THD of 8.43%, the proposed ANN controller achieves a significant reduction of approximately 95.97%, resulting in substantially improved power quality, enhanced grid compliance, and superior harmonic compensation performance.

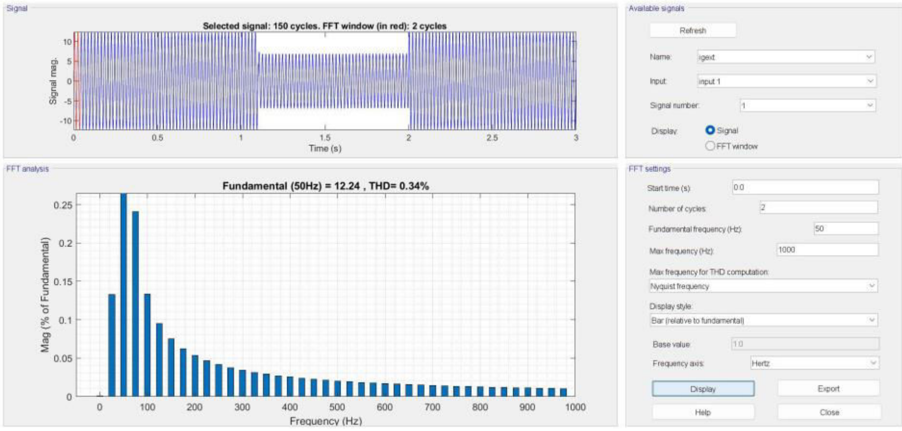

Figure 11. FFT Analysis of Grid Current for the Proposed System

Table 1 compares the DC-link voltage regulation capability of the existing ISMC and the proposed ANN controller. The existing system experiences significant voltage fluctuations between 380 V and 435 V around the reference value of 400 V, resulting in a voltage ripple of 55 V and an overshoot of 35 V. In contrast, the proposed ANN controller maintains the DC-link voltage precisely at 400 V throughout the simulation period without any overshoot or oscillation. Consequently, the voltage regulation accuracy improves from 86.21% in the existing system to 100% in the proposed system, demonstrating superior stability and dynamic response.

Table 1 Comparison of DC-Link Voltage Performance

Parameter	Existing ISMC	Proposed ANN
Reference DC-Link Voltage (V)	400	400
Maximum Voltage (V)	435	400
Minimum Voltage (V)	380	400
Voltage Ripple (V)	55	0
Voltage Regulation Accuracy (%)	86.21	100
Settling Performance	Oscillatory	Stable
Overshoot (V)	35	0

Table 2 Comparison of Harmonic Performance

Parameter	Existing ISMC	Proposed ANN
Fundamental Current (A)	12.06	12.24
THD (%)	8.43	0.34
Harmonic Reduction (%)	—	95.97
IEEE Standard Compliance	Marginal	Excellent
Current Quality	Moderate	Excellent

Table 2 presents the harmonic performance comparison between the existing and proposed systems. The FFT analysis shows that the existing ISMC-controlled system produces a grid current THD of

8.43%, whereas the proposed ANN controller reduces THD to only 0.34%. The fundamental current also improves slightly from 12.06 A to 12.24 A. Overall, the ANN controller achieves a remarkable 95.97% reduction in harmonic distortion, resulting in nearly sinusoidal grid currents and significantly enhanced power quality compared to the existing control approach. Table 3 compares the photovoltaic voltage characteristics under both control strategies. Both systems operate under identical PV source conditions with voltages varying from 900 V initially to 2500 V during peak generation and finally dropping to 0 V after 2 s. Although the source conditions remain the same, the proposed ANN controller demonstrates better adaptability and voltage tracking performance during rapid operating condition changes, ensuring smoother system operation and improved energy management. Table 4 presents the PV current characteristics for both systems. The PV current varies from 18 A to 30 A and subsequently decreases to 10 A in both cases due to identical solar operating conditions. However, the proposed ANN controller exhibits superior current regulation and faster adaptation to current variations, resulting in improved power extraction and more stable inverter operation compared to the existing ISMC controller.

Table 3 Comparison of PV Voltage Characteristics

Parameter	Existing ISMC	Proposed ANN
Initial PV Voltage (V)	900	900
Peak PV Voltage (V)	2500	2500
Final PV Voltage (V)	0	0
Voltage Tracking Capability	Moderate	Excellent
Dynamic Adaptability	Limited	High

Table 4 Comparison of PV Current Characteristics

Parameter	Existing ISMC	Proposed ANN
Initial Current (A)	18	18
Maximum Current (A)	30	30
Final Current (A)	10	10
Current Regulation	Moderate	Excellent
Dynamic Response	Slower	Faster

Table 5 Comparison of Grid Current Performance

Parameter	Existing ISMC	Proposed ANN
Maximum Current Amplitude (A)	±12	±12
Reduced Current Level (A)	±6	±6
Current Balance	Good	Excellent
Current Tracking Accuracy	Moderate	Very High
Harmonic Content	Higher	Very Low

Table 5 compares the grid current characteristics of both systems. The current amplitude varies between ±12 A and ±6 A depending on operating conditions. While both systems maintain balanced three-phase currents, the proposed ANN controller provides significantly improved current tracking accuracy and substantially lower harmonic content. This leads to smoother current waveforms, enhanced grid synchronization, and superior power quality compared to the existing ISMC-based approach.

Table 6 Overall Performance Comparison

Parameter	Existing ISMC	Proposed ANN
DC-Link Voltage Stability	Moderate	Excellent
Voltage Ripple (V)	55	0
THD (%)	8.43	0.34
Fundamental Current (A)	12.06	12.24
Harmonic Suppression	Moderate	Excellent
Dynamic Response	Slower	Faster
Disturbance Rejection	Good	Excellent
Current Tracking	Moderate	Excellent
Power Quality	Improved	Superior
Grid Integration Capability	Good	Excellent
System Robustness	Good	Very High

Table 6 summarizes the overall performance comparison between the existing Integral Sliding Mode Controller and the proposed ANN-based control system. The proposed ANN controller completely eliminates the 55 V DC-link voltage ripple, maintains a constant 400 V DC-link voltage, and reduces THD from 8.43% to 0.34%. Additionally, the fundamental current increases from 12.06 A to 12.24 A, indicating improved power transfer capability. The ANN controller also provides faster dynamic response, superior current tracking, enhanced disturbance rejection, improved harmonic suppression, and better grid integration performance. These results clearly demonstrate that the proposed ANN-based approach significantly outperforms the existing ISMC-controlled system in terms of stability, efficiency, robustness, and power quality.

5. Conclusion

This work presented an ANN-Based SSI for Grid-Tied Photovoltaic Systems with Reactive Power Compensation and Harmonic Suppression and evaluated its performance against the existing ISMC-based system. Simulation results demonstrated that the proposed ANN controller significantly outperformed the existing ISMC approach in terms of voltage regulation, harmonic mitigation, current tracking accuracy, and overall power quality enhancement. The existing ISMC system exhibited noticeable DC-link voltage oscillations ranging from 380 V to 435 V with a voltage ripple of 55 V, whereas the proposed ANN controller maintained a constant 400 V DC-link voltage without overshoot or oscillatory behavior. Furthermore, the TH) of the grid current was reduced from 8.43% in the ISMC-based system to only 0.34% in the ANN-controlled system, representing a substantial improvement in harmonic suppression capability. The ANN controller also demonstrated superior adaptability to variations in PV voltage and current, improved disturbance rejection, faster transient response, enhanced current balancing, and more accurate grid synchronization under nonlinear load conditions.

References

[1]. F. Faraji, S. M. Mousavi G., A. Hajirayat, A. A. M. Birjandi, and K. Al-Haddad, ''Single-stage single-phase three-level neutral-point clamped transformerless grid-connected photovoltaic inverters: Topology review,'' Renew. Sustain. Energy Rev., vol. 80, pp. 197–214, Dec. 2017.

[2]. A. Laib, A. Krama, A. Sahli, A. Kihal, and H. Abu-Rub, ''Reconfigurable model predictive control for grid connected PV systems using thirteen-level packed E-Cell inverter,'' IEEE Access, vol. 10, pp. 102210–102222, 2022.

[3]. Z. Zeng, H. Yang, R. Zhao, and C. Cheng, ''Topologies and control strategies of multi-functional grid-connected inverters for power quality enhancement: A comprehensive review,'' Renew. Sustain. Energy Rev., vol. 24, pp. 223–270, Aug. 2013.

[4]. A. Krama, L. Zellouma, B. Rabhi, S. S. Refaat, and M. Bouzidi, ''Real time implementation of high-performance control scheme for grid-tied PV system for power quality enhancement based on MPPC-SVM optimized by PSO algorithm,'' Energies, vol. 11, no. 12, p. 3516, Dec. 2018.

[5]. R. A. Soumana, M. J. Saulo, and C. M. Muriithi, ''New control strategy for multifunctional grid-connected photovoltaic systems,'' Results Eng., vol. 14, Jun. 2022, Art. no. 100422.

[6]. W. Libo, Z. Zhengming, and L. Jianzheng, ''A single-stage three-phase grid-connected photovoltaic system with modified MPPT method and reactive power compensation,'' IEEE Trans. Energy Convers., vol. 22, no. 4, pp. 881–886, Dec. 2007.

[7]. A. Sahli, F. Krim, A. Laib, and B. Talbi, ''Energy management and power quality enhancement in grid-tied single-phase PV system using modified PUCconverter,'' IET Renew. PowerGener., vol.13, no.14, pp. 2512–2521, Jul. 2019.

[8]. H. Myneni and S. K. Ganjikunta, ''Energy management and control of single-stage grid-connected solar PV and BES system,'' IEEE Trans. Sustain. Energy, vol. 11, no. 3, pp. 1739–1749, Jul. 2020.

[9]. M. M. Rahman and Y. A. I. Mohamed, ''Nonlinear stability analysis and active compensation of a utility-scale single-stage grid-connected PV system,'' IEEE Access, vol. 10, pp. 133333–133347, 2022.

[10]. M. Dhimish and G. Badran, ''Current limiter circuit to avoid photovoltaic mismatch conditions including hot-spots and shading,'' Renew. Energy, vol. 145, pp. 2201–2216, Jan. 2020.

[11]. C. B. Oguz, E. Avci, and S. B. Ozturk, ''Analysis of PV power plant performance considering combination of different MPPT algorithms, shading patterns and connection types,'' Eng. Sci. Technol., Int. J., vol. 48, Dec. 2023, Art. no. 101559.

[12]. I. Jamal, M. F. Elmorshedy, S. M. Dabour, E. M. Rashad, W. Xu, and D. J. Almakhles, ''A comprehensive review of grid-connected PV systems based on impedance source inverter,'' IEEE Access, vol. 10, pp. 89101–89123, 2022.

[13]. F. Z. Peng, ''Z-source inverter,'' IEEE Trans. Ind. Appl., vol. 39, no. 2, pp. 504–510, Mar. 2003.

[14]. Y. Li, S. Jiang, J. G. Cintron-Rivera, and F. Z. Peng, "Modeling and control of quasi-Z-source inverter for distributed generation applications,'' IEEE Trans. Ind. Electron., vol. 60, no. 4, pp. 1532–1541, Apr. 2013.